Chemical Papers (2021) 75:1521–1533
https://doi.org/10.1007/s11696-020-01407-8

ORIGINAL PAPER

Investigation of encapsulation of Talzenna drug into carbon and boron-nitride nanotubes [CNT(8,8-7) and BNNT(8,8-7)]: a DFT study

Fatemeh Azarakhshi[1] · Masoome Sheikhi[2] · Siyamak Shahab[3,4,5] · Mehrnoosh Khaleghian[6] · Kseniya Sirotsina[3] · Hanna Yurlevich[3] · Darya Novik[3]

Received: 20 August 2020 / Accepted: 26 October 2020 / Published online: 9 November 2020

Abstract

The aim of this work is a study of the encapsulation and intermolecular non-bonded interaction of an anticancer drug Talzenna into carbon nanotube [CNT(8,8-7)] and boron nitride nanotube [BNNT(8,8-7)]. The interaction effects of Talzenna with the CNT and BNNT on electronic and adsorption properties were theoretically investigated in the solvent phase at the M062X/6-311G* level of theory. With the encapsulation of Talzenna drug, the electronic properties of the CNT and BNNT nanotubes change significantly. The electronic spectra of the Talzenna drug, complexes CNT/Talzenna and BNNT/Talzenna in the solvent water were calculated by Time-Dependent Density Functional Theory (TD-DFT) for the study of adsorption effect. According to the natural bond orbital (NBO) results, all three molecules Talzenna, CNT and BNNT play as electrons donor and acceptors at the complexes CNT/Talzenna and BNNT/Talzenna. On the other hand, the charge transfer is occurred between the bonding, antibonding or nonbonding orbitals in molecules Talzenna, CNT and BNNT. Based on the results, CNT(8,8-7) and BNNT(8,8-7) can be used as a drug delivery system for the transportation of Talzenna as anticancer drug within the biological systems.

Keywords Talzenna · CNT(8,8-7) · BNNT(8,8-7) · DFT · NBO

Introduction

Carbon nanotubes (CNTs) are drug delivery systems applicable in biology and medicine (Padma and Jain 2014; Bae et al. 2013). CNTs can deliver anticancer drugs into target cells through penetrating to cell membranes. After

Electronic supplementary material The online version of this article (https://doi.org/10.1007/s11696-020-01407-8) contains supplementary material, which is available to authorized users.

✉ Fatemeh Azarakhshi
f_azarakhshi@yahoo.com

Masoome Sheikhi
m.sheikhi2@gmail.com

Siyamak Shahab
siyamak.shahab@yahoo.com

Mehrnoosh Khaleghian
mehr_khaleghian@yahoo.com

Kseniya Sirotsina
zmeenosec15@gmail.com

Hanna Yurlevich
ann.yurlevich@gmail.com

Darya Novik
novik301199@gmail.com

[1] Department of Chemistry, Varamin-Pishva Branch, Islamic Azad University, Varamin, Iran

[2] Young Researchers and Elite Club, Gorgan Branch, Islamic Azad University, Gorgān, Iran

[3] Belarusian State University, ISEI BSU, Minsk, Republic of Belarus

[4] Institute of Physical Organic Chemistry, National Academy of Sciences of Belarus, 13 Surganov Str., 220072 Minsk, Republic of Belarus

[5] Institute of Chemistry of New Materials, National Academy of Sciences of Belarus, 36 Skarina Str., 220141 Minsk, Republic of Belarus

[6] Department of Chemistry, Islamshahr Branch, Islamic Azad University, Islamshahr, Iran

the interaction of drug with the surface of CNTs, they are delivered into the target cells (Kumar et al. 2017). CNTs are used to improve the pharmaceutical properties. The medicinal properties of drugs improve with interaction of drug on surface of CNTs and, therefore, the toxic effect of drugs decrease (Chakrabarti et al. 2015; Foldvari 2010). Therefore, the various researches have been carried out on the Boron nitride nanostructures. These materials are applicable in electronics devices, semiconductor with high thermal stability and nanowires. The energy gap of Boron nitride nanostructure is about 6 eV. The energy gap of Boron nitride nanotubes (BNNTs) is about 5.5 eV (Golberg et al. 2007). They have nontoxic property due to their high chemical and structural stability and high oxidation resistance, along with uniformity and stability in dispersion in solution (Yu et al. 2009).

Talazoparib with trade name Talzenna (Fig. 1) has been developed by the United States Food and Drug Administration (FDA) for use in treatment advanced breast cancer (Exman et al. 2019). Talzenna acts as an inhibitor of poly-ADP ribose polymerase (PARP) which aids in single-strand DNA repair (Huang et al. 2015; Murai et al. 2012, 2014). Talzenna was confirmed in 2018 in the United States and 2019 in the Europe for advanced or metastatic breast cancer treatment (Exman et al. 2019; Domchek et al. 2019).

Performing Density functional theory (DFT) calculations, one may obtain useful information about the interaction between various nanotubes and drug molecules. The adsorption and interaction of anticancer drugs, such as cisplatin (Feazell et al. 2007), carboplatin (Dhar et al. 2008), paclitaxel (Liu et al. 2008), methotrexate (Pastorin et al. 2006) and doxorubicin (Ali-Boucetta et al. 2008) with BNNT, have already been studied. We have already studied the interaction between a new azomethine derivative and BN(6,6-7) nanotube by DFT calculations (Sheikhi et al. 2017). We discussed on the electronic properties, chemical shift tensors, electronic spectra natural charge of the azomethine and BN(6,6-7) nanotube in the complex BN(6,6-7)/azomethine. Recently, we have also investigated the adsorption and non-bonded interaction between various drugs, such as Syndros (Sheikhi et al. 2018a), Resveratrol (Sheikhi et al. 2018b), Alectinib (Sheikhi et al. 2019a), Rubraca (Sheikhi et al. 2019b), Curcumin (Shahab et al. 2019a) and Tyrphostin AG528 (Sheikhi et al. 2019c), over a variety of carbon nanotubes. In the current study, the encapsulation of Talzenna into the CNT(8,8-7) and BNNT(8,8-7) has been investigated by DFT method. We have studied changes in geometric parameters, thermodynamic parameters, frontier molecular orbitals (FMOs), quantum-chemical molecular descriptors, charge transfer analysis according to natural bond orbital (NBO) analysis and electronic structure and excited states.

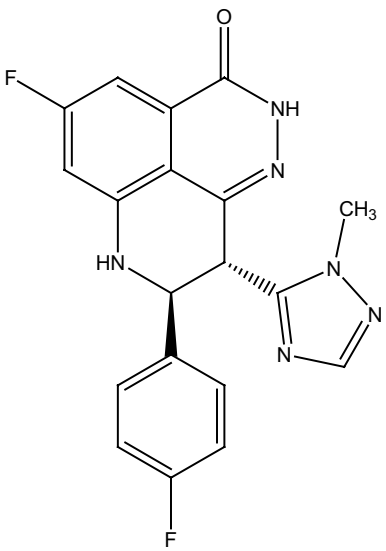

Fig. 1 Chemical structure of Talzenna

Computational methods and equipment

In this work, we have studied the encapsulation and non-bonded interaction between Talzenna drug with the CNT(8,8-7) and BNNT(8,8-7) by computational research. The quantum chemical calculations have been performed using the density functional theory (DFT) at the M062X method and 6-311G* basis set (Yoosefian and Jahani 2019; Rahmani et al. 2019) by the Gaussian 09 W program (Frisch et al. 2009) for the optimization of the molecule Talzenna drug, CNT(8,8-7), BNNT(8,8-7) and complexes CNT/Talzenna and BNT/Talzenna. The Polarized Continuum Model (PCM) (Frisch et al. 2009) was used for the calculations of solvent effect. The adsorption energies (E_{ad}) (Sheikhi et al. 2018a) of Talzenna drug over CNT and BNNT are obtained by the following equations:

$$E_{ad} = E_{CNT/Talzenna} - [E_{Talzenna} + E_{CNT}] \quad (1)$$

$$E_{ad} = E_{BNNT/Talzenna} - [E_{Talzenna} + E_{BNNT}] \quad (2)$$

in which $E_{CNT/Talzenna}$ and $E_{BNNT/Talzenna}$ are the adsorption energies of the Talzenna on the carbon nanotube and BN nanotube, respectively. E_{BNNR} and E_{AlNNR} are energies of the BNNR(8,8-7) and AlNNR(8,8-7), respectively. Also, $E_{Talzenna}$ is the energy of Talzenna molecule.

Geometrical parameters, thermodynamic parameters, NBO analysis (Shahab et al. 2017a), density of states (DOS), and FMO analysis (Sheikhi et al. 2018c) were calculated using M062X/6-311G* level of theory. The molecular orbital (MO) calculations of the title compounds, such as

E_{HOMO}, E_{LUMO}, energy gap between LUMO and HOMO ($E_g = E_{LUMO} - E_{HOMO}$), were computed. The optimized molecular structures, DOS results and the molecular orbitals's graphs were visualized by and GaussView program (Shahab et al. 2017b). TD-DFT method (Frisch et al. 2000) was used for the calculation of electronic transitions of the Talzenna drug and the complexes CNT/Talzenna and BNNT/Talzenna. UV–Vis experimental absorption spectra of the complexes were measured by Cary 60 UV–Vis scanning spectrophotometer.

Results and discussion

Optimized structures

We calculated the optimized structures of the Talzenna drug, CNT(8,8-7), and BNNT(8,8-7) using DFT method in a solvent water. These structures are shown in Fig. 2.

In the first step, we have considered five states for encapsulation of the Talzenna into the CNT(8,8-7) and BNNT(8,8-7). The optimized states (S1, S2, S3, S4, S5) of the CNT(8,8-7) and BNNT(8,8-7) were calculated at the PM6 method (Fig. 3). The energies (E) for the investigated states S1, S2, S3, S4, and S5 are reported in Table 1. The calculated energies show that the most stable state of CNT(8,8-7) and BNNT(8,8-7) is state S5.

Consequently, we have considered the encapsulation of the Talzenna into the CNT(8,8-7) and BNNT(8,8-7) at the state S5 and have optimized using M062X/6-311G* level of theory in a solvent water. The optimized structures are shown in Figs. 4, 5.

Geometrical parameters play an important role to illustrate the adsorption of the molecules on nanotubes in drug delivery systems. The calculated selective bond lengths of the optimized structures of Talzenna, CNT(8,8-7), BNNT(8,8-7), complexes CNT(8,8-7)/Talzenna and BNNT(8,8-7)/Talzenna at the interacting locations are reported in Tables S1 and S2 (Atoms numbering is according to Figs. 4, 5). As shown in Tables S1 and S2, some geometrical parameters of Talzenna drug, carbon and BN nanotube are changed after the intermolecular non-bonded interaction drug with nanotubes and the formation of the complex, although these changes are not significant.

The thermochemical parameters, such as the sum of electronic and thermal energies ($E+T$), the sum of electronic and thermal enthalpies ($E+H$), the sum of electronic and thermal free energies ($E+G$), and entropy (S) of the Talzenna drug, CNT(8,8-7), BNNT(8,8-7), complexes CNT/Talzenna and BNNT/Talzenna, calculated using M062X/6-311G* level of theory. The results were reported in Table 2. With the encapsulation of the Talzenna drug in CNT(8,8-7) and BNNT(8,8-7), the Thermal, Gibbs and Enthalpy energies values decrease. The computed energy values show the reduced reactivity and increasing the stability of Talzenna drug in non-bonded interaction with CNT(8,8-7) and BNNT(8,8-7). The calculated energies for the complex BNNT/Talzenna are more negative rather than the complex CNT/Talzenna; also, the relative values of energies for BNNT/Talzenna are smaller than CNT/Talzenna; therefore, the complex BNNT/Talzenna has the most stability comparing with the complex CNT/Talzenna.

Electronic properties

The HOMO and LUMO orbitals (FMO) have a significant role in the chemical reactions and charge transfer phenomenon in molecules (Sheikhi et al. 2018a; Shahab et al. 2018). The HOMO and LUMO energies display the ability of orbital to donate and obtain an electron, respectively (Sheikhi et al. 2018b). The energy gap between HOMO and LUMO orbitals is a major factor in designation the electrical

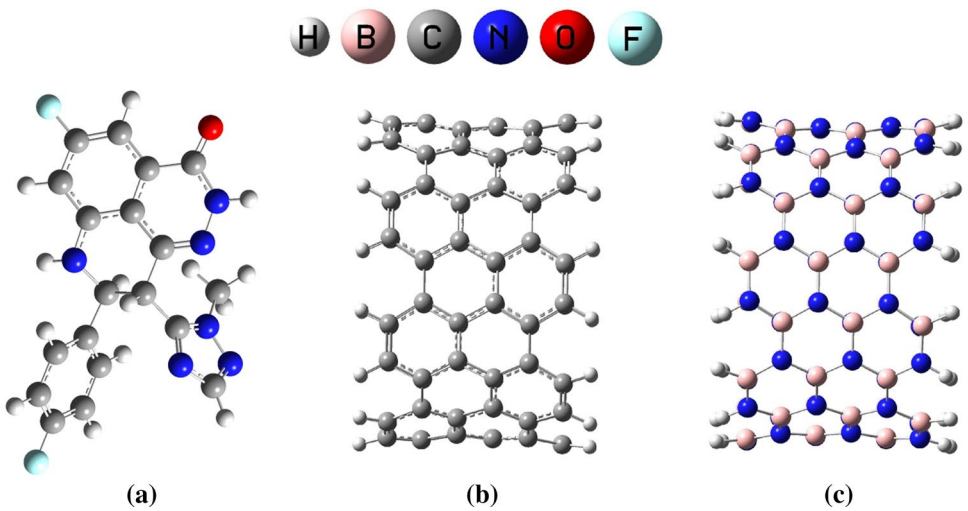

Fig. 2 The optimized geometry of the molecules **a** Talzenna, **b** CNT(8,8-7), **c** BNNT(8,8-7) using M062X/6-311G* level of theory

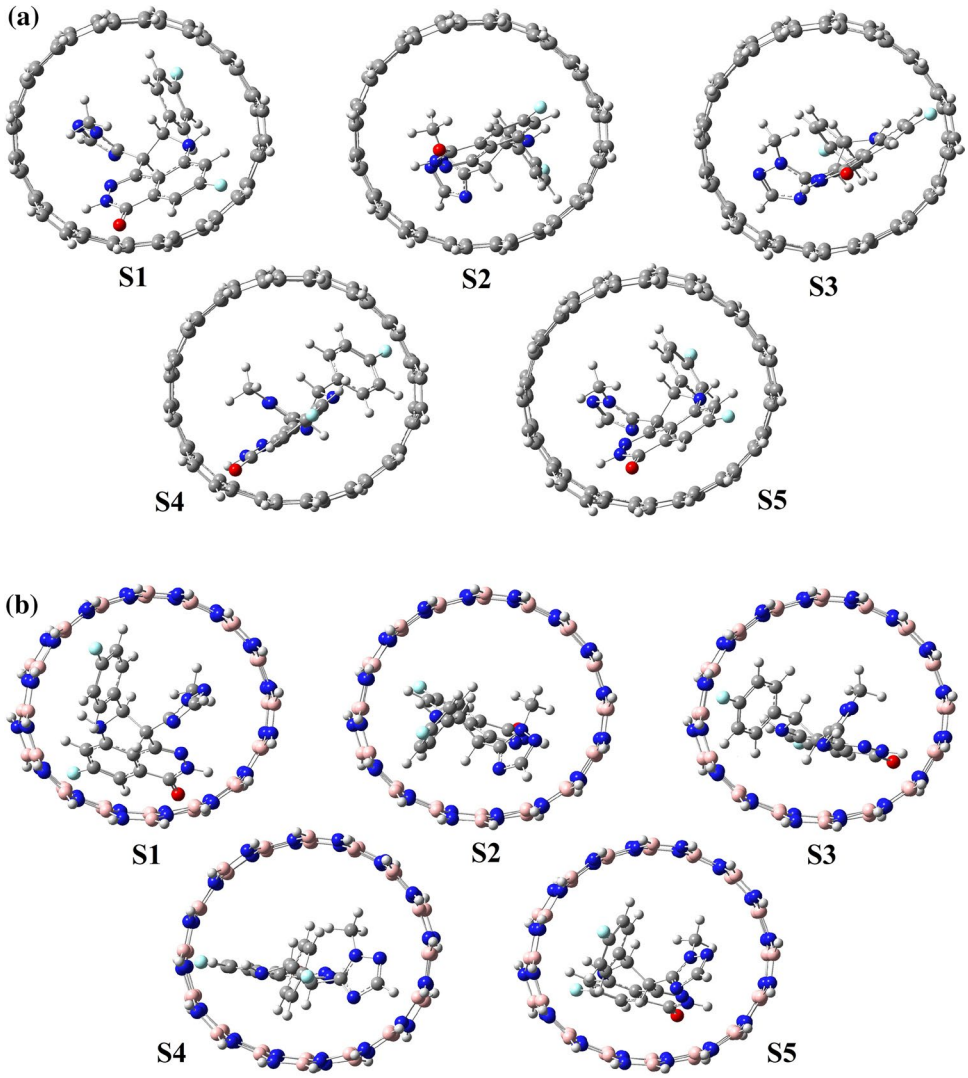

Fig. 3 The encapsulated states of the compound Talzenna into the CNT(8,8-7) and BNNT(8,8-7) optimized by PM6 method; **a** CNT/Talzenna, **b** BNNT/Talzenna

Table 1 The calculated energies (E) for states S1, S2, S3, S4, and S5 of the CNT(8,8-7) and BNNT(8,8-+7) by PM6 method

Compounds	Different orientation	*E* (Hartree)
CNT/Talzenna	S1	− 3.8089491
	S2	− 3.9011544
	S3	− 2.7631164
	S4	− 3.7579248
	S5	− 4.0961959
BNNT/Talzenna	S1	0.8214085
	S2	1.3704191
	S3	1.101003
	S4	2.0731128
	S5	0.70178

transport properties in molecules (Sheikhi et al. 2018c). We have investigated the non-bonded intermolecular interaction effects between Talzenna drug with CNT(8,8-7) and BNNT(8,8-7) on the electronic properties. The calculated results are reported in Table 3.

The adsorption energies (E_{ad}) of the Talzenna drug over the CNT(8,8-7) and BNNT(8,8-7) are computed about − 40.78 eV and − 36.39 eV, respectively; therefore, the encapsulation of the Talzenna drug on the CNT(8,8-7) and BNNT(8,8,-7) is exothermic (Table 3). The adsorption energy of the Talzenna drug on the CNT(8,8-7) is greater than the adsorption energy of the Talzenna drug on the BNNT(8,8-7). Thus, it indicated a strong adsorption in complex CNT/Talzenna rather than BNNT/Talzenna complex.

After the encapsulation of Talzenna into CNT(8,8-7), the energies of HOMO and LUMO are decreased from − 5.81 and − 2.54 eV in carbon nanotube to − 5.82 and − 2.56 eV, respectively, in the complex CNT/Talzenna. The energy of HOMO is increased from − 8.11 eV in BNNT to − 7.65 eV in the complex BNNT/Talzenna, whereas the energy of LUMO is decreased from 0.65 eV to − 1.04 eV. The frontier orbitals graphs of the molecules Talzenna, CNT(8,8-7),

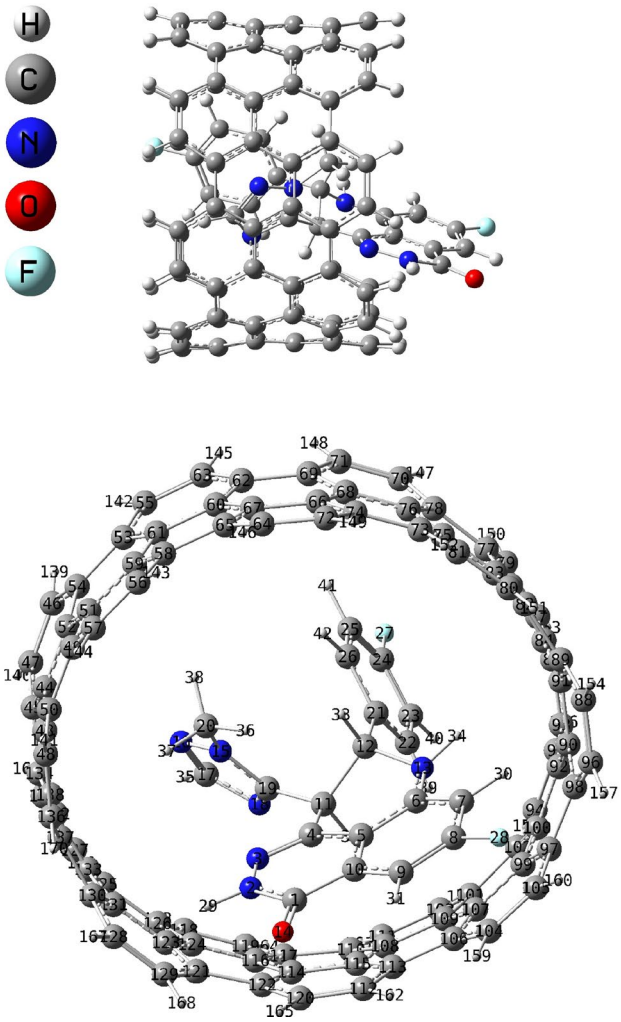

Fig. 4 The optimized geometry of the complex CNT/Talzenna using M062X/6-311G* level of theory

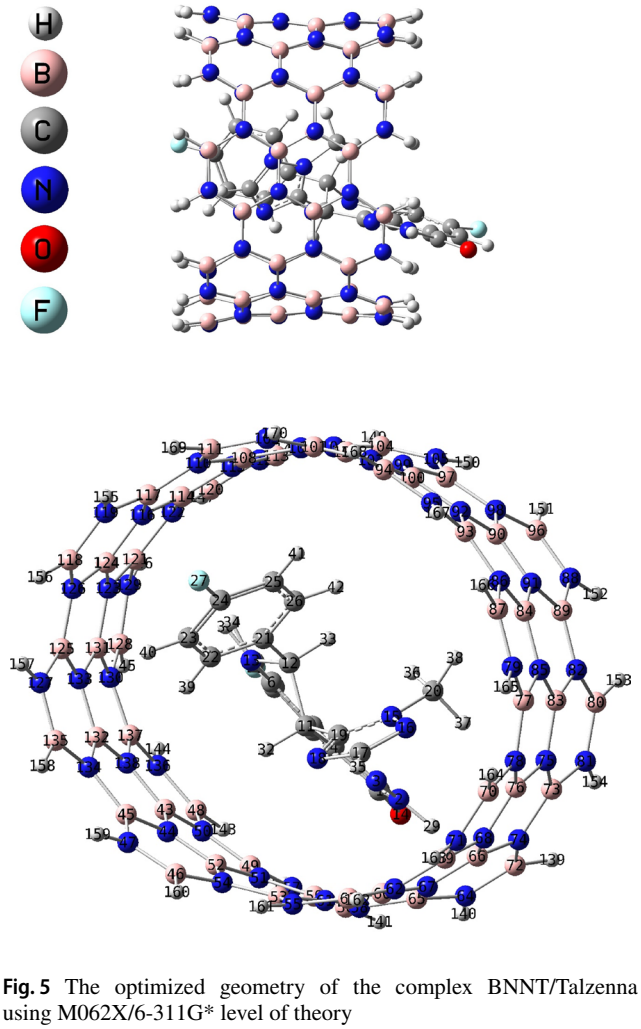

Fig. 5 The optimized geometry of the complex BNNT/Talzenna using M062X/6-311G* level of theory

BNNT(8,8-7), CNT/Talzenna and BNNT/Talzenna are presented in Fig. 6. Figure 6 shows that the electron density of HOMO and LUMO orbitals in the CNT(8,8-7) is mainly localized on the double bonds C=C of carbon nanotube. The HOMO orbital of the BNNT(8,8-7) mainly situated on nitrogen atoms, whereas the LUMO orbital localized on boron atoms. The electron density of HOMO and LUMO orbitals in the CNT(8,8-7)/Talzenna is mainly localized on the double bonds C=C of carbon nanotube, while the electron density of HOMO and LUMO orbitals in the BNNT(8,8-7)/Talzenna is mainly localized on the Talzenna drug.

The energy gaps values of the title molecules are reported in Table 3. The calculated DOS plots (Shahab et al. 2019b) in Fig. 7 also display the energy gaps of the investigated compounds. According to results of Table 3, the energy gaps are decreased from 3.27 and 7.46 eV in CNT and BNNT to 3.26 and 6.61 eV in the complexes CNT/Talzenna and BNNT/Talzenna, respectively. These results show increase in electrical conductivity of the complexes rather than the pure CNT and BNNT. Thus, we found that the CNT can be a better nanotube for encapsulation of the Talzenna drug due to the lower energy gap (3.27 eV) rather than BNNT (7.46 eV).

The quantum molecular descriptors for the investigated compounds including ionization potential (I), electron affinity (A), global hardness (η), electronegativity (χ), electronic chemical potential (μ), electrophilicity (ω) and chemical softness (S) are computed according to following equations, respectively (Shahab et al. 2019c):

$$\left[I = -E_{HOMO}\right], \left[A = -E_{LUMO}\right], \left[\eta = I\text{-}A/2\right],$$
$$\left[\chi = I + A/2\right], \left[\mu = -(I + A)/2\right], \left[\omega = \mu^2/2\eta\right], \left[S = 1/2\eta\right]$$

in which are summarized in Table 3. The stability of the molecules is determined to hardness factor that shows chemical reactivity (Shahab et al. 2019d). According to Table 3, the values of global hardness (η) for CNT and BNNT are 1.63 eV and 3.73 eV. After capsulation of Talzenna drug

Table 2 The thermochemical parameters of the molecules Talzenna, CNT(8,8-7), BNNT(8,8-7), and complexes CNT/Talzenna and BNNT/Talzenna and relative values of energies calculated by M062X/6-311G* level of theory

Parameters	Talzenna	CNT(8,8-7)	BNNT(8,8-7)	CNT/Talzenna	BNNT/Talzenna
$E+G$ (Hartree)	− 1335.443	− 3676.381	− 3844.522	− 5011.860	− 5179.994
$E+H$ (Hartree)	− 1335.370	− 3676.251	− 3844.372	− 5011.684	− 5179.800
$E+T$ (Hartree)	− 1335.371	− 3676.252	− 3844.373	− 5011.684	− 5179.801
S (cal/mol.K)	153.617	274.563	317.037	370.912	408.182
$\Delta G_{adsorption}$	–	–	–	− 0.036	− 0.029
$\Delta H_{adsorption}$	–	–	–	− 0.063	− 0.058

Table 3 The calculated electronic properties of the Talzenna drug, CNT(8,8-7), BNNT(8,8-7) and the complexes CNT/Talzenna and BNNT/Talzenna at the M062X/6-311G* level of theory in the solvent water

Property	Talzenna	CNT(8,8-7)	BNNT(8,8-7)	CNT/Talzenna	BNNT/Talzenna
Dipole moment (Debye)	5.470	0.031	0.005	5.633	5.565
E(Hartree)	− 1335.711	− 3677.258	− 3845.313	− 5013.034	− 5181.082
E_{HOMO} (eV)	− 7.51	− 5.81	− 8.11	− 5.82	− 7.65
E_{LUMO} (eV)	− 0.87	− 2.54	0.65	− 2.56	− 1.04
E_g (eV)	6.64	3.27	7.46	3.26	6.61
E_{ads} (eV)	–	–	–	− 40.78	− 36.39
I (eV)	7.51	5.81	8.11	5.82	7.65
A (eV)	0.87	2.54	0.65	2.56	1.04
χ (eV)	4.19	4.17	4.38	4.19	4.34
η (eV)	3.32	1.63	3.73	1.63	3.30
μ (eV)	− 4.19	− 4.17	− 4.38	− 4.19	− 4.34
ω (eV)	2.64	5.33	2.57	5.38	2.85
S (eV)	0.15	0.31	0.13	0.31	0.15

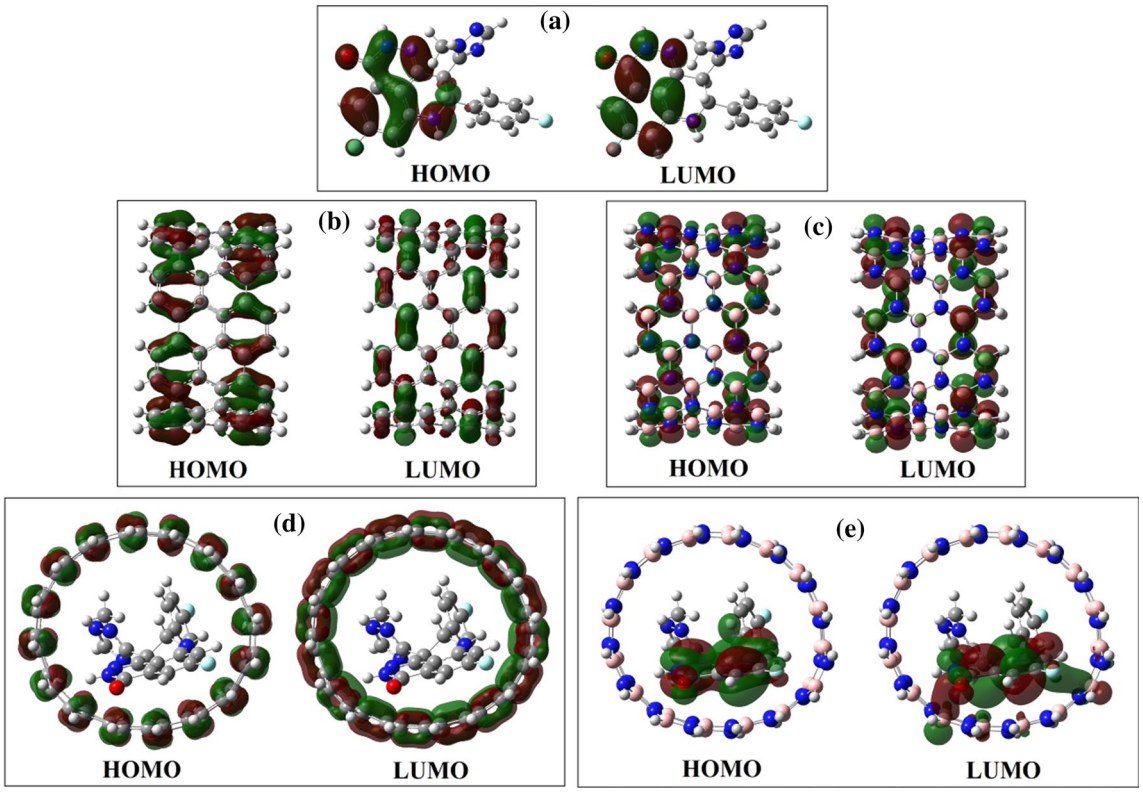

Fig. 6 The calculated HOMO, LUMO orbitals **a** the Talzenna drug, **b** CNNT(8,8-7), **c** BNNT(8,8-7), **d** the complex CNT/Talzenna, and **e** the complex BNNT/Talzenna at the M062X/6-311G* level of theory

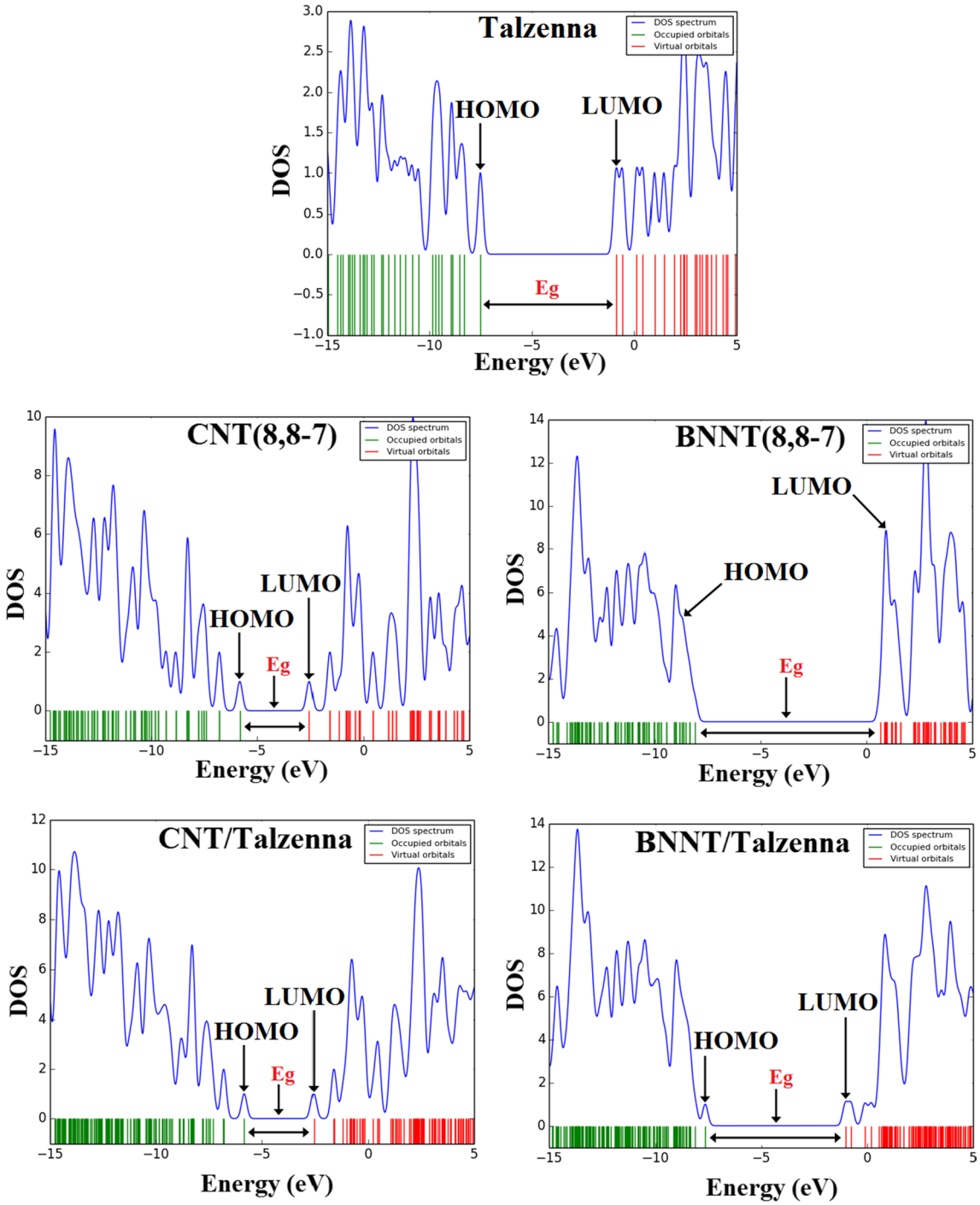

Fig. 7 DOS plots of the Talzenna drug, CNNT(8,8-7), BNNT(8,8-7) and the complexes CNT/Talzenna and BNNT/Talzenna using M062X/6-311G* level of theory

into CNT and BNNT, the global hardness of in complex CNT/Talzenna has not changed (1.63 eV), whereas the global hardness of complex BNNT/Talzenna decreases to 3.30 eV. Also, the reactivity of CNT is the higher rather than BNNT due to the low η of CNT (1.63 eV) comparing with the η of BNNT (3.73 eV) that shows CNT is more reactive than BNNT. The electronic chemical potential (μ) index of the complexes CNT/Talzenna and BNNT/Talzenna also decreased rather than the pure CNT and BNNT. Therefore, the complexes have a high chemical activity, low chemical stability and, therefore, they are a soft system.

The amount of dipole moment CNT(8,8-7) is increased after capsulation of Talzenna drug from 0.031 Debye to 5.633 Debye in complex CNT/Talzenna and the amount of dipole moment of BNNT(8,8-7) is increased after interaction with Talzenna from 0.005 Debye to 5.565 Debye in complex BNNT/Talzenna (see Table 3). The change of dipole moment after encapsulation of Talzenna drug into carbon and BN nanotubes displays a charge transfer between Talzenna drug and the title nanotubes.

NBO analysis

NBO analysis is an important method for studying intra- and inter-molecular bonding and interaction between bonds in molecular systems (Sheikhi et al. 2018d). The electron delocalization from donor orbitals (full NBOs) to acceptor orbitals (empty NBOs) describes a conjugative electron transfer process between them (Sheikhi et al. 2018d). For each donor orbital (i) and acceptor orbital (j), the stabilization energy $E^{(2)}$ associated with the delocalization $i \rightarrow j$ is calculated by the following equation (Weinhold and Landis 2001):

$$E^{(2)} = \Delta E_{ij} = q_i \frac{F(ij)^2}{e_j - e_i} \quad (4)$$

The stabilization energy ($E^{(2)}$) describes the amount of the participation of electrons in the resonance between atoms of the molecular structure (Frisch et al. 2009). The bigger $E^{(2)}$, the more donation tendency from electron donor orbital to electron acceptor orbital (Sheikhi et al. 2018d). The NBO analysis for complex CNT/Talzenna and BNNT/Talzenna has been performed by M062X/6-311G* level of theory and the results are summarized in Tables S3 and S4 (Atoms numbering is according to Figs. 4, 5).

The $\sigma \rightarrow \pi^*$, $\pi \rightarrow \pi^*$ and $\pi^* \rightarrow \pi^*$ transitions from Talzenna to CNT(8,8-7) occur in complex CNT/Talzenna. According to results of NBO analysis in Table S3, the $\sigma \rightarrow \pi^*$ transitions from Talzenna to CNT(8,8-7) take place as σ(N2-H29) → π*(C128–C129) and σ(C7–H30) → π*(C88–C96) with stabilization energies ($E^{(2)}$) about 0.11, 0.14 kcal/mol, respectively. The $\pi \rightarrow \pi^*$ transitions are, such as π(N3–C4) → π*(C114–C122), π(C1–C5) → π*(C104–C105), π(C1–C5) → π*(C112–C120), π(C6–C7) → π*(C88–C96), π(C6–C7) → π*(C104–C105), π(C22–C23) → π*(C86–C87), interactions with resonance energies ($E^{(2)}$) about 0.13, 0.12, 0.25, 0.15, 0.25, 0.13 kcal/mol, respectively. The important $n \rightarrow \pi^*$ transition is observed for n1(N2) → π*(C112–C120) and n1(N2) → π*(C128–C129) interactions with stabilization energies ($E^{(2)}$) about 0.44, 0.53 kcal/mol, respectively. According to results of Table S3, the $\pi^* \rightarrow \pi^*$ transitions have the highest resonance energies comparing with other transitions from Talzanna to CNT(8,8-7) including π*(N3–C4) → π*(C112–C120), π*(N3-C4) → π*(C121-C123), π*(C6-C7) → π*(C104-C105), π*(N16-C17) → π*(C125-C127), π*(N16-C17) → π*(C132-C133) with stabilization energies ($E^{(2)}$) about 1.04, 1.35, 1.77, 1.82, 2.12 kcal/mol, respectively. The NBO analysis shows that $\pi \rightarrow \sigma^*$ transitions from CNT(8,8-7) to Talzenna occur in complex CNT/Talzenna. The main $\pi \rightarrow \sigma^*$ electron charge transfer is observed for π(C88–C96) → σ*(C7–H30), π(C94–C95) → σ*(C23–H40), π(C128–C129) → σ*(N2–H29) with high stabilization energies ($E^{(2)}$) 0.91, 0.50 and 0.98 kcal/mol, respectively. Thus, Talzenna and CNT(8,8-7) act as both electron donor and electron acceptor and charge transfer takes place between Talzenna and CNT(8,8-7) in the complex CNT/Talzenna.

The NBO analysis shows that $\sigma \rightarrow \pi^*$, $\pi \rightarrow \pi^*$, $n \rightarrow \pi^*$ transitions from Talzenna to BNNT(8,8-7) occur in complex BNNT/Talzenna (Table S4). As shown in Table S4, the important $\sigma \rightarrow \pi^*$ transitions from Talzenna to BNNR(8,8-7) take place as σ(C20–H37) → π*(B73–N74), σ(C20–H38) → π*(N75–B83), σ(C22-H39) → π*(B132–N133), σ(C25-H41) → π*(B101-N102), with resonance energies ($E^{(2)}$) about 1.16, 0.98, 1.38, 1.64 kcal/mol, respectively. The $\pi \rightarrow \pi^*$ transitions from Talzenna to BNNT(8,8-7) are, such as π(N2–H29) → π*(B56–N57), π(N3–C4) → π*(B49–N51), π(N16–C17) → π*(B60–N67), π(N16–C17) → π*(N62–B69), π(N16–C17) → π*(N68–B76), interactions with stabilization energies ($E^{(2)}$) about 0.87, 0.66, 0.37, 0.73 and 0.64 kcal/mol, respectively. The important $n \rightarrow \pi^*$ charge transfers from Talzenna to BNNT(8,8-7) are observed for n1(N2) → π*(B56–N57), n1(N3) → π*(N58–B65), n1(N16) → π*(N68–B76), n1(N16) → π*(B77–N78), n1(N18) → π*(B53–N55) interactions with stabilization energies ($E^{(2)}$) about 2.75, 2.24, 4.22, 1.01, 1.12 kcal/mol, respectively. Also, the $\pi \rightarrow \sigma^*$, $\pi \rightarrow \pi^*$ and $\pi^* \rightarrow \pi^*$ transitions from BNNT(8,8-7) to Talzenna occur in complex BNNT/Talzenna. According to the results of NBO analysis, the important interactions from BNNT(8,8-7) to Talzenna are, such as π(N64-B72) → σ*(N2-H29), π(B121-N129) → σ*(C7-H30), π*(B121-N129) → σ*(N13-H34), π*(B132-N133) → σ*(C22-H39), transitions with stabilization energies values ($E^{(2)}$) of 2.81, 0.85, 0.61, 0.88 kcal/mol, respectively. Thus, Talzenna and BNNR(8,8-7) act as both electron donor and electron acceptor in the complex BNNT/Talzenna and, therefore, charge transfer takes place between Talzenna and BNNT(8,8-7).

Electronic Structure and Excited States

To investigate encapsulation effect of Talzenna into CNT(8,8-7) and BNNT(8,8-7) on the λ_{max}, we have obtained

the theoretical UV/Vis spectra of Talzenna and the complexes CNT/Talzenna and BNNT/Talzenna using TD-DFT calculations at M062X/6-311G* method. We investigated 20 excited states and reported the important transitions in Tables 4, 5, 6. Tables 4, 5 and 6 show the λ_{max}, oscillator strength (f), and excitation energies (E). In the calculated UV spectrum of Talzenna drug, λ_{max} appears at 159.55 nm ($f=0.94$) (Table 4). The charge transfer at $\lambda_{max}=159.55$ nm is related to the excited state $S_0 \rightarrow S_{12}$ with eight electron configurations, such as H-5 → L + 1 (35%), H-3 → L + 2 (15%), H-4 → L + 1 (6%), H-2 → L + 1 (5%), H-2 → L + 5 (5%), H-1 → L + 3 (9%), H → L (4%), H → L + 5 (7%), in which the main transition is the transition from HOMO-5 to LUMO + 1 [H-5 → L + 1 (35%)]. The excited state of $S_0 \rightarrow S_{14}$ at 154.41 nm (f = 0.61) is also the other important excited state in the UV spectrum of Talzenna. The other excited states of Talzenna drug have a small intensity. The calculated UV spectrum of Talzenna drug in the solvent water is displayed on Fig. 8.

With the encapsulation of Talzenna into the CNT(8,8-7), λ_{max} is appeared at 365.71 nm ($f=1.39$) in electronic absorption spectrum of complex CNT(8,8-7) that is due to charge transfer of one electron into the excited state $S_0 \rightarrow S_3$ and it describes by three configurations for one-electron excitation H-2 → L (38%), H → L + 2 (37%), H → L + 1 (3%) (Table 5). The main transition is including the transition from HOMO-2 to LUMO [H-2 → L (38%)]. The excited state of $S_0 \rightarrow S_2$ at 371.57 nm ($f=1.27$) is also the other important excited state in the theoretical UV/Vis spectrum of the complex CNT/Talzenna. The other excited states of CNT/Talzenna have very small intensity and do not play any role in the formation of electron spectrum of the title complex (Table 5). The theoretical UV spectrum of CNT/Talzenna in the solvent water displayed on in Fig. 8.

After the encapsulation of Talzenna into the BNNT(8,8-7), λ_{max} appears at 162.44 nm ($f=0.47$) in the calculated UV spectrum of BNNT/Talzenna. The charge transfer at $\lambda_{max}=162.44$ nm is related to the excited state $S_0 \rightarrow S_{11}$ and

Table 4 Electronic absorption spectrum of Talzenna drug calculated by TDM062X/6-311G* method

Excited State	Wavelength (nm)	Excitation Energy (eV)	Configurations Composition (corresponding transition orbitals)	Oscillator Strength (f)
$S_0 \rightarrow S_1$	244.53	5.07	H → L (84%), H-5 → L + 1 (2%), H → L + 1 (4%)	0.23
$S_0 \rightarrow S_2$	224.76	5.51	H-2 → L (15%), H → L + 1 (62%), H-1 → L (4%), H → L (6%)	0.22
$S_0 \rightarrow S_7$	191.39	6.47	H-2 → L (48%), H-1 → L (19%), H → L + 1 (21%), H-4 → LUMO (2%)	0.48
$S_0 \rightarrow S_8$	185.13	6.69	H-2 → L + 1 (52%), H-1 → L + 1 (18%), H → L + 5 (12%), H-5 → L + 5 (2%), H → L (2%)	0.32
$S_0 \rightarrow S_9$	164.69	7.52	H-5 → L (68%), H-6 → L (2%), H-4 → L (6%), H-4 → L + 4 (6%), H → L + 1 (4%)	0.47
$S_0 \rightarrow S_{10}$	162.38	7.63	H-4 → L + 4 (55%), H-3 → L + 2 (11%), H-6 → L + 6 (3%), H-5 → L (4%), H-3 → L + 4 (3%), H-2 → L + 4 (6%), H-1 → L + 3 (5%)	0.51
$S_0 \rightarrow S_{12}$	159.55	7.77	H-5 → L + 1 (35%), H-3 → L + 2 (15%), H-4 → L + 1 (6%), H-2 → L + 1 (5%), H-2 → L + 5 (5%), H-1 → L + 3 (9%), H → L (4%), H → L + 5 (7%)	0.94
$S_0 \rightarrow S_{13}$	155.25	7.98	H-5 → L + 1 (15%), H-3 → L + 2 (22%), H-1 → L + 3 (16%)H-5 → L (3%), H-4 → L + 1 (2%), H-4 → L + 4 (9%), H-3 → L + 3 (2%), H-2 → L + 3 (3%), H-1 → L + 1 (4%), H → L + 5 (7%)	0.24
$S_0 \rightarrow S_{14}$	154.41	8.02	H-3 → L + 3 (54%), H-1 → L + 2 (25%), H-4 → L + 3 (2%), H-3 → L + 1 (6%), H-2 → L + 2 (5%)	0.61

Table 5 Electronic absorption spectrum of complex CNT/Talzenna calculated by TDM062X/6-311G* method

Excited State	Wavelength (nm)	Excitation Energy (eV)	Configurations Composition (corresponding transition orbitals)	Oscillator Strength **(f)**
$S_0 \rightarrow S_2$	371.57	3.33	H-1 → L (39%), H → L + 1 (38%), H → L + 2 (3%)	1.27
$S_0 \rightarrow S_3$	365.71	3.39	H-2 → L (38%), H → L + 2 (37%), H → L + 1 (3%)	1.39

*In this Table the transitions with $f \geq 0.10$ are presented

**H* HOMO, *L* LUMO

Table 6 Electronic absorption spectrum of complex BNNT/Talzenna calculated by TDM062X/6-311G* method

Excited State	Wavelength (nm)	Excitation Energy (eV)	Configurations Composition (corresponding transition orbitals)	Oscillator Strength (*f*)
$S_0 \rightarrow S_1$	243.28	5.09	H → L (81%), H → L + 1 (5%)	0.19
$S_0 \rightarrow S_2$	225.26	5.50	H-3 → L (15%), H → L + 1 (55%), H-2 → L (3%), H-1 → L (3%), H → L (7%)	0.12
$S_0 \rightarrow S_7$	191.66	6.46	H-3 → L (39%), H-1 → L (10%), H → L + 1 (24%), H-2 → L (8%)	0.44
$S_0 \rightarrow S_8$	186.75	6.63	H-3 → L + 1 (44%), H-1 → L + 1 (10%), H-2 → L + 1 (8%), H → L (2%), H → L + 15 (4%)	0.25
$S_0 \rightarrow S_9$	166.89	7.42	H-24 → L (17%), H-22 → L (28%), H-26 → L (3%), H-20 → L (9%), H-13 → L (3%), H-11 → L + 4 (3%), H-10 → L (2%), H → L + 1 (3%)	0.27
$S_0 \rightarrow S_{10}$	165.05	7.51	H-13 → L + 4 (12%), H-11 → L + 4 (19%), H-22 → L (2%), H-10 → L + 4 (9%), H-9 → L + 4 (2%), H-7 → L + 2 (9%), H-3 → L + 4 (5%), H-1 → L + 3 (3%)	0.25
$S_0 \rightarrow S_{11}$	162.44	7.63	H-22 → L + 1 (13%), H-7 → L + 2 (14%), H-24 → L + 1 (8%), H-20 → L + 1 (4%), H-13 → L + 1 (2%), H-3 → L + 1 (5%), H-2 → L + 3 (3%), H-1 → L + 3 (7%), H → L (3%), H → L + 15 (3%)	0.47
$S_0 \rightarrow S_{13}$	158.27	7.83	H-7 → L + 3 (31%)H-22 → L + 1 (3%), H-7 → L + 1 (3%), H-7 → L + 2 (8%), H-6 → L + 3 (3%), H-3 → L + 2 (5%), H-2 → L + 2 (4%), H-1 → L + 1 (4%), H-1 → L + 2 (9%), H-1 → L + 3 (2%)	0.19
$S_0 \rightarrow S_{14}$	157.55	7.86	H-7 → L + 3 (12%)H-24 → L + 1 (3%), H-22 → L + 1 (5%), H-11 → L + 4 (3%), H-7 → L + 1 (4%), H-7 → L + 2 (9%), H-3 → L + 3 (4%), H-2 → L + 2 (3%), H-2 → L + 3 (3%), H-1 → L + 2 (6%), H-1 → L + 3 (7%)	0.13

*In this Table the transitions with $f \geq 0.10$ are presented

**H* HOMO, *L* LUMO

is defined by ten configurations including H-22 → L + 1 (13%), H-7 → L + 2 (14%), H-24 → L + 1 (8%), H-20 → L + 1 (4%), H-13 → L + 1 (2%), H-3 → L + 1 (5%), H-2 → L + 3 (3%), H-1 → L + 3 (7%), H → L (3%), H → L + 15 (3%) (Table 6). Excitation of an electron from H-7 → L + 2 (14%) gives the main contribution to the formation of the absorption band at 162.44 nm. The other important excited state is excitation of one electron at 191.66 nm ($f = 0.44$) that belonged to the transition into the excited state $S_0 \rightarrow S_7$. The other excited states of the title complex have small intensity. The calculated UV spectrum of the complex BNNT/Talzenna displayed on in Fig. 8.

In the UV spectrum of isolated Talzenna drug, λ_{max} appeared at 159.55 nm, while after encapsulation of Talzenna into CNT(8,8-7) and BNNT(8,8-7) is changed to 365.71 nm and 162.44 nm, respectively. According to these results, we found that encapsulation of Talzenna drug into CNT and BNNT enhances the value of λ_{max} and it can be recognized as a bathochromic shift.

Conclusion

In this work, we have studied the adsorption energies and electronic properties of capsulation of Talzenna drug into CNT(8,8-7) and BNNT(8,8-7) using DFT calculations and UV/Vis spectroscopy investigations. The results show that Talzenna drug has the higher adsorption energy (-40.78 eV) with CNT rather than BNNT (36.39 eV). The CNT(8,8-7) with the lower energy gap (3.27 eV) rather than the BNNT (7.46 eV) can be a better choice for encapsulation of the Talzenna drug. Also, the values of η parameter of CNT (1.63 eV) and BNNT (3.73 eV) specified that the reactivity of CNT is higher rather than BNNT that shows the Talzenna increasing the reactivity of CNT comparing with BNNR. NBO analysis predicted a charge transfer from the Talzenna drug to CNT and BNNT and from CNT and BNNT to Talzenna. The encapsulation of Talzenna drug into the CNT and BNNT increases the value of λ_{max} (from 159.55 nm to 365.71 nm in CNT/Talzenna and from 159.55 nm to

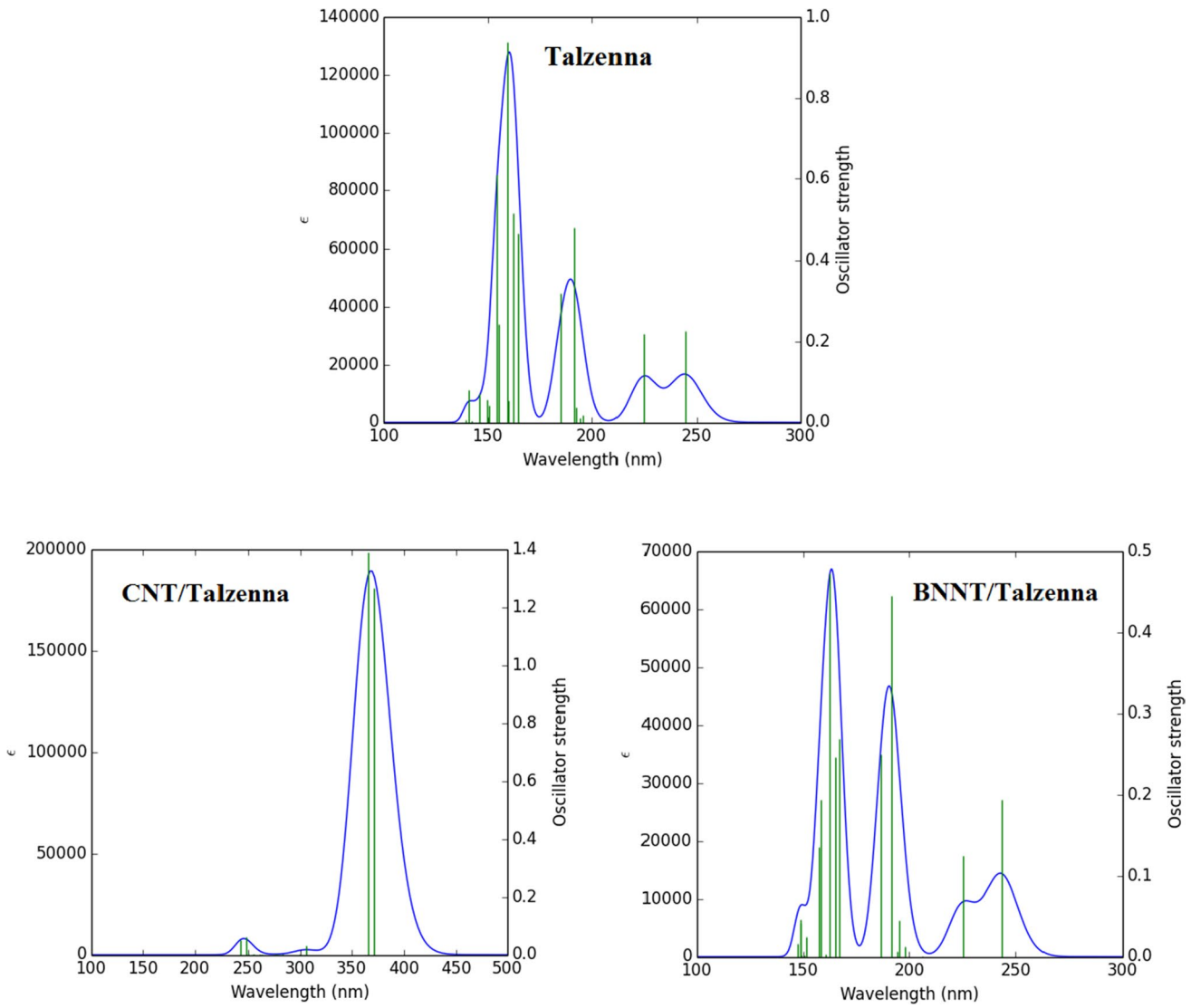

Fig. 8 UV spectrum of the Talzenna drug (**a**), complex CNT/Talzenna (**b**) and BNNT/Talzenna (**c**) calculated by TDM062X/6-311G* method

162.44 nm in BNNT/Talzenna) and it can be considered as a bathochromic shift. We hope that results of our research can be used in drugs delivery to cancer cells and to support decreased drug interaction with healthy tissue.

References

Ali-Boucetta H, Al-Jamal KT, McCarthy D, Prato M, Bianco A, Kostarelos K (2008) Multiwalled carbon nanotube-doxorubicin supramolecular complexes for cancer therapeutics. Chem Comm 4:459–461. https://doi.org/10.1039/B712350G

Bae YH, Mrsny RJ, Park K (eds) (2013) Cancer targeted drug delivery: an elusive dream. Springer Science & Business Media.

Chakrabarti M, Kiseleva R, Vertegel A, Ray SK (2015) Carbon nanomaterials for drug delivery and cancer therapy. J Nanosci Nanotechnol 15:5501–5511. https://doi.org/10.1166/jnn.2015.10614

Dhar S, Liu Z, Thomale J, Dai H, Lippard SJ (2008) Targeted single-wall carbon nanotube-mediated Pt(IV) prodrug delivery using folate as a homing device. J Am Chem Soc 130:11467–21176. https://doi.org/10.1021/ja803036e

Domchek S, Postel-Vinay S, Im SA, Park YH, Delord JP, Italiano A, Alexandre J, You B, Bastian S, Krebs MG, Waqar S, Lanasa M, Angell HK, Tang M, Gresty C, Opincar L, Herbolsheimer P, Kaufman B (2019) Abstract PD5–04: an open-label, phase II basket study of olaparib and durvalumab (MEDIOLA): updated results in patients with germline BRCA-mutated (gBRCAm) metastatic breast cancer (MBC). Cancer Res 79:PD5–04. https://doi.org/10.1158/1538-7445.SABCS18-PD5-04

Exman P, Barroso-Sousa R, Tolaney SM (2019) Evidence to date: talazoparib in the treatment of breast cancer. Onco Targets Ther 12:5177–5187. https://doi.org/10.2147/OTT.S184971

Feazell RP, Nakayama-Ratchford N, Dai H, Lippard SJ (2007) Soluble single-walled carbon nanotubes as longboat delivery systems for platinum (iv) anticancer drug design. J Am Chem Soc 129:8438–8439. https://doi.org/10.1021/ja073231f

Foldvari M (2010) Formulating nanomedicines: focus on carbon nanotubes as novel nanoexcipients. Key engineering materials. Trans Tech Publ 441:53–74. https://doi.org/10.4028/www.scientific.net/KEM.441.53

Frisch A, Nielson AB, Holder AJ (2000) GAUSSVIEW User Manual. Gaussian Inc., Pittsburgh

Frisch MJ, Trucks GW, Schlegel HB, Scuseria GE, Robb MA, Cheeseman JR, Scalmani G, Barone V, Mennucci B, Petersson GA, Nakatsuji H, Caricato M, Li X, Hratchian HP, Izmaylov AF, Bloino J, Zheng G, Sonnenberg JL, Hada M, Ehara M, Toyota K, Fukuda R, Hasegawa J, Ishida M, Nakajima T, Honda Y, Kitao O, Nakai H, Vreven T, Montgomery JA, Peralta JE, Ogliaro F, Bearpark M, Heyd JJ, Brothers E, Kudin KN, Staroverov VN, Kobayashi R, Normand J, Raghavachari K, Rendell A, Burant JC, Iyengar SS, Tomasi J, Cossi M, Rega N, Millam JM, Klene M, Knox JE, Cross JB, Bakken V, Adamo C, Jaramillo J, Gomperts R, Stratmann RE, Yazyev O, Austin AJ, Cammi R, Pomelli C, Ochterski JW, Martin RL, Morokuma K, Zakrzewski VG, Voth GA, Salvador P, Dannenberg JJ, Dapprich S, Daniels AD, Farkas O, Foresman JB, Ortiz JV, Cioslowski J, Fox DJ (2009) Gaussian 09 revision A02. Gaussian Inc, Wallingford CT

Golberg D, Bando Y, Tang CC, Zhi CY (2007) Boron nitride nanotubes. Adv Mater 19:2413–2432. https://doi.org/10.1002/adma.200700179

Huang J, Wang L, Cong Z, Amoozgar Z, Kiner E, Xing D, Orsulic S, Matulonis U, Goldberg MS (2015) The PARP1 inhibitor BMN 673 exhibits immunoregulatory effects in a Brca1−/− murine model of ovarian cancer. Biochem Biophys Res Commun 463:5551–556. https://doi.org/10.1016/j.bbrc.2015.05.083

Kumar B, Jalodia K, Kumar P, Gautam HK (2017) Recent advances in nanoparticle-mediated drug delivery. J Drug Deliv Sci Technol 41:260–268. https://doi.org/10.1016/j.jddst.2017.07.019

Liu Z, Chen K, Davis C, Sherlock S, Cao Q, Chen X, Dai H (2008) Drug delivery with carbon nanotubes for in vivo cancer treatment. Cancer Res 68:6652–6660. https://doi.org/10.1158/0008-5472.CAN-08-1468

Murai J, Huang SYN, Das BB, Renaud A, Zhang Y, Doroshow JH, Ji J, Takeda S, Pommier Y (2012) Trapping of PARP1 and PARP2 by clinical PARP inhibitors. Cancer Res 72:5588–5599. https://doi.org/10.1158/0008-5472.CAN-12-2753

Murai J, Huang SY, Renaud A, Zhang Y, Ji J, Takeda S, Morris J, Teicher B, Doroshow JH, Pommier Y (2014) Stereospecific PARP trapping by BMN 673 and comparison with olaparib and rucaparib. Mol Cancer Ther 13:433–443. https://doi.org/10.1158/1535-7163.MCT-13-0803

Padma VD, Jain S (eds) (2014) Targeted drug delivery: concepts and design advances in delivery science and technology. Springer.

Pastorin G, Wu W, Wieckowski S, Briand JP, Kostarelos K, Prato M, Bianco A (2006) Double functionalisation of carbon nanotubes for multimodal drug delivery. Chem Comm 11:1182–1184. https://doi.org/10.1039/B516309A

Rahmani Z, Edjlali L, Vessally E, Hosseinian A, Delir Kheirollahi Nezhad P (2019) A density functional theory outlook on the possible sensing ability of boron nitride nanotubes and their Al- and Si-doped derivatives for sulfonamide drugs. J Sulfur Chem 41:82–95. https://doi.org/10.1080/17415993.2019.1687702

Shahab S, Filippovich L, Sheikhi M, Kumar R, Dikusar E, Yahyaei H, Muravsky A (2017) Polarization, excited states, trans-cis properties and anisotropy of thermal and electrical conductivity of the 4-(phenyldiazenyl)aniline in PVA matrix. J Mol Struct 1141:703–709. https://doi.org/10.1016/j.molstruc.2017.04.014

Shahab S, Sheikhi M, Filippovich L, Dikusar Anatol'evich E, Yahyaei H (2017) Quantum chemical modeling of new derivatives of (E, E)-azomethines: synthesis, spectroscopic (FT-IR, UV/Vis, polarization) and thermophysical investigations. J Mol Struct 1137:335–348. https://doi.org/10.1016/j.molstruc.2017.02.056

Shahab S, Sheikhi M, Filippovich L, Khaleghian M, Dikusar E, Yahyaei H, Yousefzadeh Borzehandani M (2018) Spectroscopic studies (geometry optimization, E→ZIsomerization, UV/Vis, excited states, FT-IR, HOMO-LUMO, FMO, MEP, NBO, Polarization) and anisotropy of thermal and electrical conductivityof new azomethine dyes in stretched polymer matrix. Silicon 10:2361–2385. https://doi.org/10.1007/s12633-018-9773-8

Shahab S, Sheikhi M, Khaleghian M, Balakhanava I, Azarakhshi F (2019) DFT Study of Physisorption Effect of the Curcumin on CNT(8,0-6) Nanotube for Biological Applications. Chin J Struct Chem 38:37–52. https://doi.org/10.14102/j.cnki.0254-5861.2011-2052.

Shahab S, Sheikhi M, Khaleghian M, Kaviani S (2019) Theoretical study of interaction between apalutamide anticancer drug and thymine by DFT method. Chin J Struct Chem 3s8:1645–1663. https://doi.org/10.14102/j.cnki.0254-5861.2011-2282

Shahab S, Sheikhi M, Filippovich L, Dikusar E, Rouhani M, Pazniak A, Kumar R (2019) Molecular investigations of the new synthesized azomethines as antioxidants: theoretical and experimental studies. Current Mol Med 19:419–433. https://doi.org/10.2174/1566524019666190509102620

Shahab S, Sheikhi M, Filippovich L, Ignatovich Z, Muravsky A, Alnajjar R, Kaviani S, Strogova A (2019) Optimization, Spectroscopic (FT-IR, Excited States, UV/Vis) Studies, FMO, ELF, LOL, QTAIM and NBO analyses and electronic properties of two new pyrimidine derivatives. Chin J Struct Chem 38:1615–1639. https://doi.org/10.14102/j.cnki.0254-5861.2011-2251

Sheikhi M, Shahab S, Filippovich L, Khaleghian M, Dikusar E, Mashayekhi M (2017) Interaction between new synthesized derivative of (E, E)-azomethines and BN(6,6–7) nanotube for medical applications: geometry optimization, molecular structure, spectroscopic (NMR, UV/Vis, excited state), FMO, MEP and HOMO-LUMO investigations. J Mol Struct 1146:881–888. https://doi.org/10.1016/j.molstruc.2017.06.017

Sheikhi M, Shahab S, Khaleghian M, Kumar R (2018) Interaction between new anti-cancer drug syndros and CNT (6, 6–6) nanotube for medical applications: geometry optimization, molecular structure, spectroscopic (NMR, UV/Vis, Excited state), FMO, MEP and HOMO-LUMO investigation. Appl Surf Sci 434:504–513. https://doi.org/10.1016/j.apsusc.2017.10.154

Sheikhi M, Shahab S, Khaleghian M, Hajikolaee FH, Balakhanava I, Alnajjar R (2018) Adsorption properties of the molecule resveratrol on CNT (8, 0–10) nanotube: geometry optimization, molecular structure, spectroscopic (NMR, UV/Vis, Excited State), FMO, MEP and HOMO-LUMO investigations. J Mol Struct 1160:479–478. https://doi.org/10.1016/j.molstruc.2018.01.005

Sheikhi M, Shahab S, Filippovich L, Yahyaei H, Dikusar E, Khaleghian M (2018) New derivatives of (E, E)-azomethines: Design, quantum chemical modeling, spectroscopic (FT-IR, UV/Vis, polarization) studies, synthesis and their applications: experimental and theoretical investigations. J Mol Struct 1152:368–385. https://doi.org/10.1016/j.molstruc.2017.09.108

Sheikhi M, Shahab S, Filippovich L, Dikusar E, Khaleghian M (2018) DFT investigations (geometry optimization, UV/Vis, FT-IR, NMR, HOMO-LUMO, FMO, MEP, NBO, Excited States) and synthesis of new pyrimidine dyes. Chin J Struc Chem 37:1201–1222. https://doi.org/10.14102/j.cnki.0254-5861.2011-1887

Sheikhi M, Shahab S, Alnajjar R, Ahmadianarog M (2019) Adsorption properties of the new anti-cancer drug alectinib on

CNT(6,6–6) nanotube: geometry optimization, molecular structure, spectroscopic (NMR, UV/Vis, Excited State), FMO, MEP and HOMO-LUMO investigations. J clust sci 30:83–96. https://doi.org/10.1007/s10876-018-1460-9

Sheikhi M, Shahab S, Khaleghian M, Ahmadianarog M, Kumar R (2019) Investigation of the adsorption rubraca anticancer drug on the CNT(4,4–8) nanotube as a factor of drug delivery: a theoretical study based on DFT method. Curr Mol Med 19:473–486. https://doi.org/10.2174/1566524019666190506143152

Sheikhi M, Shahab S, Alnajjar R, Ahmadianarog M, Kaviani S (2019) Investigation of adsorption tyrphostin AG528 anticancer drug upon the CNT(6,6–6) nanotube: a DFT study. Curr Mol Med 19:91–104. https://doi.org/10.2174/1566524019666190226111823

Weinhold F, Landis CR (2001) Natural Bond Orbitals and Extensions of Localized. Chem Educ Res Pract 2:91–104. https://doi.org/10.1039/B1RP90011K

Yoosefian M, Jahani M (2019) A molecular study on drug delivery system based on carbon nanotube for the novel norepinephrine prodrug, Droxidopa. J Mol Liq 284:258–264. https://doi.org/10.1016/j.molliq.2019.04.016

Yu J, Chen Y, Cheng BM (2009) Dispersion of boron nitride nanotubes in aqueous solution with the help of ionic surfactants. Solid State Commun 149:763–766. https://doi.org/10.1016/j.ssc.2009.03.001